

Generalized Optimal Classification Trees: A Mixed-Integer Programming Approach

Jiancheng Tu^a, Wenqi Fan^{a, b}, Zhibin Wu^c

^a Department of Computing, The Hong Kong Polytechnic University, jiancheng.tu@connect.polyu.hk; ^b Department of Management and Marketing, The Hong Kong Polytechnic University, wenqi.fan@polyu.edu.hk; ^c Business School, Sichuan University, Chengdu 610065, P R China, zhibinwu@scu.edu.cn

Authors are encouraged to submit new papers to INFORMS journals by means of a style file template, which includes the journal title. However, use of a template does not certify that the paper has been accepted for publication in the named journal. INFORMS journal templates are for the exclusive purpose of submitting to an INFORMS journal and are not intended to be a true representation of the article's final published form. Use of this template to distribute papers in print or online or to submit papers to another non-INFORMS publication is prohibited.

Abstract. Global optimization of decision trees is a long-standing challenge in combinatorial optimization, yet such models play an important role in interpretable machine learning. Although the problem has been investigated for several decades, only recent advances in discrete optimization have enabled practical algorithms for solving optimal classification tree problems on real-world datasets. Mixed-integer programming (MIP) offers a high degree of modeling flexibility, and we therefore propose a MIP-based framework for learning optimal classification trees under nonlinear performance metrics, such as the F1-score, that explicitly addresses class imbalance. To improve scalability, we develop problem-specific acceleration techniques, including a tailored branch-and-cut algorithm, an instance-reduction scheme, and warm-start strategies. We evaluate the proposed approach on 50 benchmark datasets. The computational results show that the framework can efficiently optimize nonlinear metrics while achieving strong predictive performance and reduced solution times compared with existing methods.

Key words: Interpretable machine learning, Optimal classification tree, Imbalanced classification, Mixed-integer programming, Branch and cut

1. Introduction

Decision trees occupy a central role in interpretable machine learning, valued for their inherent transparency and ease of explanation. The classical Classification and Regression Trees (CART) algorithm (Breiman et al. 1984) exemplifies the dominant paradigm: tree structures are constructed via recursive, greedy splitting rules. Although such heuristics are computationally attractive, they provide no guarantee of global optimality, and the problem of finding the smallest or most accurate decision tree consistent with data is known to be NP-complete (Laurent and Rivest 1976). As a consequence, traditional practice has long relied on heuristic induction methods.

Recently, the global optimization of decision trees has attracted increasing attention, which seeks to construct tree models that are provably optimal with respect to prescribed objectives and constraints, rather than heuristic surrogates. A variety of exact approaches have been advanced, including mixed-integer programming (MIP) (Bertsimas and Dunn 2017, Verwer and Zhang 2019, Aghaei et al. 2025, Firat et al. 2020, Günlük et al. 2021, Subramanian and Sun 2023), branch-and-bound algorithms (Mazumder et al. 2022), dynamic programming (DP) (van der Linden et al. 2023, Demirović et al. 2023, 2022, Lin et al. 2020), and constraint programming (CP) (Shati et al. 2023, Narodytska et al. 2018). These efforts have convincingly demonstrated that globally optimized trees can achieve superior predictive performance and model complexity compared to greedy induction.

Among these paradigms, MIP-based approaches stand out for their modeling power: they can naturally encode a wide range of objective functions and constraints. This flexibility has motivated continued research into MIP formulations for optimal classification trees and their scalable methods.

1.1. MIP-based Approaches for Optimal Classification Trees

The foundational MIP model for optimal classification trees proposed by Bertsimas and Dunn (2017) showed that small-depth globally optimal trees could surpass classic heuristics such as CART, sparking an active line of research on improved formulations. Subsequent work has addressed issues of robustness (Bertsimas et al. 2019), stability (Bertsimas et al. 2022), and computational efficiency (Verwer and Zhang 2019, Günlük et al. 2021, Aghaei et al. 2025, Firat et al. 2020, Patel et al. 2024, Subramanian and Sun 2023, Alston et al. 2022).

For instance, the `BinOCT` framework (Verwer and Zhang 2019) leverages binary path-encoding variables to reduce model size, while Aghaei et al. (2025) introduced a max-flow-based formulation (`FlowOCT`) and a Benders decomposition approach to improve tractability for larger problems. Other contributions have examined cutting planes (Michini and Zhou 2025) and column generation methods (Firat et al. 2020, Patel et al. 2024, Subramanian and Sun 2023).

Despite these methodological advances, two core challenges persist: (i) most existing MIP frameworks can directly optimize only *linear* objectives (e.g., misclassification error, balanced accuracy), and do not accommodate inherently nonlinear metrics such as the F1-score, Fowlkes–Mallows index, or Matthews correlation coefficient; and (ii) scalability remains a significant barrier, often requiring hours to solve medium-scale instances.

1.2. Optimal Classification Trees for Imbalanced Data

Class imbalance is prevalent in many high-stakes domains such as fraud detection (Van Vlasselaer et al. 2017) and medical diagnosis (Chicco and Jurman 2020). Most optimal classification tree

formulations address imbalance by assigning class-specific misclassification weights or by maximizing balanced accuracy (Lin et al. 2020, van der Linden et al. 2023, Shati et al. 2023, Aghaei et al. 2025, Tu and Wu 2025). While such linear objectives facilitate tractable MIP formulations, they may fail to fully reflect nonlinear metrics such as F1-score and the Matthews correlation coefficient.

A number of recent works have sought to incorporate these nonlinear metrics into optimal tree learning. For example, Subramanian and Sun (2023) encode F1-score as constraints, while Tu and Wu (2025) propose a mixed-integer quadratic programming (MIQP) model to directly maximize F1-score. However, the inherent non-convexity of these formulations imposes a severe computational burden.

Dynamic programming (DP) approaches (Lin et al. 2020, van der Linden et al. 2023, Demirović and Stuckey 2021) can optimize certain nonlinear metrics under specific conditions, but are restricted to feature sets and typically require the objective to be additively or separably structured. As a result, developing scalable methods for learning globally optimal trees under nonlinear, imbalance-aware metrics remains an open and challenging problem.

1.3. Contributions

To address the limitations identified above, we develop a unified MIP framework capable of directly optimizing a broad class of nonlinear, imbalance-aware metrics—including the F1-score, Matthews correlation coefficient (MCC), and Fowlkes–Mallows index—through tractable linearizations. We further design a problem-specific branch-and-cut algorithm that leverages problem structure and feature-aware instance compression to achieve superior scalability. The principal contributions of this work are as follows:

- We propose a general MIP-based formulation for learning optimal classification trees that can directly optimize a wide range of nonlinear metrics derived from the confusion matrix, offering a principled solution to imbalanced classification.
- We introduce a customized branch-and-cut algorithm that leverages feature-aware and conflict cuts to improve scalability.
- Through extensive computational experiments on 50 benchmark datasets (ranging from 100 to 245,057 samples), we demonstrate that our framework consistently outperforms state-of-the-art methods such as BendersOCT (Aghaei et al. 2025) in terms of scalability and the dynamic programming approach of Demirović and Stuckey (2021) in terms of nonlinear objectives, delivering improved performance on imbalanced classification tasks and achieving substantial reductions in computation time.

Section 2 establishes the core formulation. Section 3 subsequently broadens the framework to handle nonlinear, imbalance-sensitive objective functions. Section 4 introduces several acceleration techniques to reduce runtime. Section 5 reports computational results, and Section 6 concludes.

2. Weighted Flow-based Optimal Classification Trees

We develop a weighted flow formulation for optimal classification trees that aggregates duplicate feature–label pairs into unique instances with integer multiplicities. Building on FlowOCT (Aghaei et al. 2025), the resulting WFlowOCT preserves optimal solutions while reducing problem size. We solve it via a Benders decomposition analogous to that employed in BendersOCT (Aghaei et al. 2025).

2.1. Problem Formulation

Consider a classification problem defined over a feature index set \mathcal{F} and a finite label set \mathcal{K} . The training data consist of binary-valued feature vectors paired with categorical labels, denoted by $\mathcal{I} = \{(\mathbf{x}_i, y_i)\}_{i=1}^{|\mathcal{I}|}$, where $\mathbf{x}_i \in \{0, 1\}^{|\mathcal{F}|}$ and $y_i \in \{0, 1, \dots, |\mathcal{K}| - 1\}$. We represent the classifier as a complete binary decision tree of maximum depth D with $T = 2^{D+1} - 1$ nodes, partitioned into branch nodes $\mathcal{B} = \{1, \dots, \lfloor T/2 \rfloor\}$ and leaf nodes $\mathcal{L} = \{\lfloor T/2 \rfloor + 1, \dots, T\}$. Let $\mathcal{V}_{\text{tree}} = \mathcal{B} \cup \mathcal{L}$ denote tree nodes. In the associated flow network (Figure 1), we use a source s and a sink t , and define $\mathcal{V} = \{s\} \cup \mathcal{V}_{\text{tree}} \cup \{t\}$.

DEFINITION 1 (UNIQUE DATASET). Let $\mathcal{U} = \{(\mathbf{x}_i, y_i)\}_{i=1}^{|\mathcal{U}|}$ be the set of unique instances obtained from \mathcal{I} by merging duplicates with identical (\mathbf{x}, y) . Let \mathcal{A} denote the set of post-discretization attributes, and for each $a \in \mathcal{A}$ let m_a be the number of admissible bins or levels (for a binary attribute, $m_a = 2$; for an attribute discretized into three bins, $m_a = 3$). Then the number of unique instances satisfies

$$|\mathcal{U}| \leq \min \left\{ |\mathcal{K}| \cdot \prod_{a \in \mathcal{A}} m_a, |\mathcal{I}| \right\}. \quad (1)$$

For each unique instance $i \in \mathcal{U}$, let $w_i \in \mathbb{Z}_{\geq 1}$ denote its frequency in \mathcal{I} ; then

$$\sum_{i \in \mathcal{U}} w_i = |\mathcal{I}|. \quad (2)$$

The unique number of instances $|\mathcal{U}|$ is much lower than the upper bound determined by Equation (1). The results are presented in Table EC.1. For example, the dataset *sepsis* contains 110,205 instances, but its unique dataset size is $|\mathcal{U}| = 140$, which is lower than its upper bound 32,768.

We adopt the standard FlowOCT graph (Figure 1) from Aghaei et al. (2025). For $n \in \mathcal{B}$, define the parent $a(n) = \lfloor n/2 \rfloor$ (with $a(1) = s$), the left child $\ell(n) = 2n$, and the right child $r(n) = 2n + 1$.

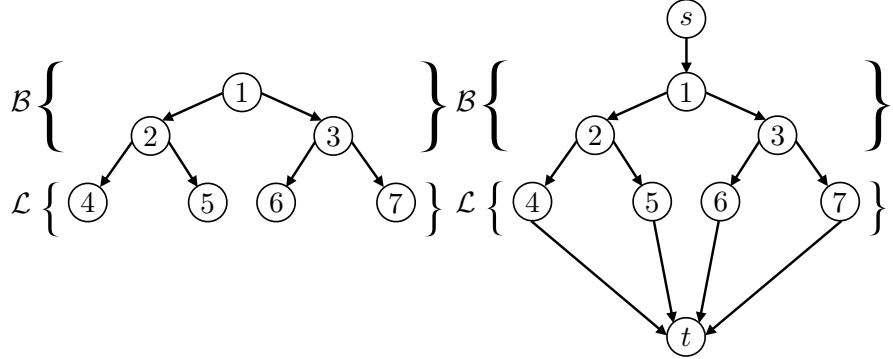


Figure 1 A depth-2 decision tree (left) and its induced flow network (right). The network is constructed by augmenting the tree nodes with a source and a sink; arcs correspond to tree edges and terminal connections from leaves to the sink. Here, $\mathcal{B} = \{1, 2, 3\}$ and $\mathcal{L} = \{4, 5, 6, 7\}$, while $\mathcal{V} = \{s, 1, 2, \dots, 7, t\}$ and $\mathcal{A} = \{(s, 1), (1, 2), \dots, (7, t)\}$ (Aghaei et al. 2025).

For any node $n \in \mathcal{V}_{\text{tree}}$, let $\mathcal{P}(n)$ denote its set of strict ancestors in \mathcal{B} . Based on the unique dataset

\mathcal{U} , we design the weighted flow formulation (WF_{LOW}OCT). We introduce the following decision

variables: $b_{nf} \in \{0, 1\}$ indicates feature f is selected to split at branch n ; $p_n \in \{0, 1\}$ indicates node

$n \in \mathcal{V}_{\text{tree}}$ is a terminal (leaf) node; $c_{nk} \in \{0, 1\}$ assigns label k to node $n \in \mathcal{V}_{\text{tree}}$; $z_{a(n),n}^i$ indicates

that data point i is correctly classified and traverses the arc $(a(n), n)$ ($=1$) or not ($=0$). For a

regularization parameter $\lambda \in [0, 1]$, the WFlowOCT model is:

$$\max (1 - \lambda) \sum_{i \in \mathcal{U}} \sum_{n \in \mathcal{V}_{\text{tree}}} w_i z_{n,t}^i - \lambda \sum_{n \in \mathcal{B}} \sum_{f \in \mathcal{F}} b_{nf} \quad (3a)$$

$$\text{s.t. } \sum_{f \in \mathcal{F}} b_{nf} + p_n + \sum_{m \in \mathcal{P}(n)} p_m = 1 \quad \forall n \in \mathcal{B} \quad (3b)$$

$$p_n + \sum_{m \in \mathcal{P}(n)} p_m = 1 \quad \forall n \in \mathcal{L} \quad (3c)$$

$$z_{a(n),n}^i = z_{n,\ell(n)}^i + z_{n,r(n)}^i + z_{n,t}^i \quad \forall n \in \mathcal{B}, \forall i \in \mathcal{U} \quad (3d)$$

$$z_{a(n),n}^i = z_{n,t}^i \quad \forall n \in \mathcal{L}, \forall i \in \mathcal{U} \quad (3e)$$

$$z_{s,1}^i \leq 1 \quad \forall i \in \mathcal{U} \quad (3f)$$

$$z_{n,\ell(n)}^i \leq \sum_{f \in \mathcal{F}: x_f^i = 0} b_{nf} \quad \forall n \in \mathcal{B}, \forall i \in \mathcal{U} \quad (3g)$$

$$z_{n,r(n)}^i \leq \sum_{f \in \mathcal{F}: x_f^i = 1} b_{nf} \quad \forall n \in \mathcal{B}, \forall i \in \mathcal{U} \quad (3h)$$

$$z_{n,t}^i \leq c_{n,y_i} \quad \forall n \in \mathcal{V}_{\text{tree}}, \forall i \in \mathcal{U} \quad (3i)$$

$$\sum_{k \in \mathcal{K}} c_{nk} = p_n \quad \forall n \in \mathcal{V}_{\text{tree}} \quad (3j)$$

$$b_{nf}, p_n, c_{nk}, z_{a(n),n}^i, z_{n,t}^i \in \{0, 1\} \quad (3k)$$

The main differences between WFlowOCT and FlowOCT lie in their objective functions and in the range of the decision variables $z_{a(n),n}^i$. The constraints of WFlowOCT are structurally similar to those of FlowOCT ; detailed formulations and explanations of the original FlowOCT constraints are provided in E-Companion EC.1. A key computational benefit of WFlowOCT arises when the number of unique instances satisfies $|\mathcal{U}| < |\mathcal{I}|$, in which case the size of the mixed-integer formulation is dramatically reduced. For instance, for the `sepsis` dataset reported in Table EC.1, the ratio $|\mathcal{I}|/|\mathcal{U}| = 110,204/140 \approx 787$ indicates that the flow-assignment components of WFlowOCT scale by only about 1/787 relative to their counterparts in FlowOCT .

PROPOSITION 1. *WFlowOCT is equivalent to FlowOCT in the sense that there exists a bijection between optimal solutions: given any optimal FlowOCT solution on \mathcal{I} , there is an optimal WFlowOCT solution on (\mathcal{U}, w) with identical tree structure and objective value, and vice versa.*

Following Aghaei et al. (2025), we adopt a Benders decomposition tailored to `WFlowOCT`. Let $g^i(\mathbf{b}, \mathbf{c}, \mathbf{p})$ denote the maximum feasible $s-t$ flow for instance $i \in \mathcal{U}$ under capacities induced by $(\mathbf{b}, \mathbf{c}, \mathbf{p})$. The master problem (MP) optimizes over the structural decision variables $(\mathbf{b}, \mathbf{c}, \mathbf{p})$, while the subproblem (SP) computes each g^i as a max-flow on the fixed network associated with instance i .

Solving the SP implies a family of standard max-flow Benders cuts. For each instance $i \in \mathcal{U}$ and each s -separating cut $\mathcal{S} \subseteq \mathcal{V} \setminus \{t\}$ with $s \in \mathcal{S}$, let $C(\mathcal{S})$ denote the set of arcs crossing the cut. Introducing variables $g^i \in \{0, 1\}$ to represent the maximum attainable flow for instance i , the resulting Benders master problem is:

$$\max (1 - \lambda) \sum_{i \in \mathcal{U}} w_i g^i - \lambda \sum_{n \in \mathcal{B}} \sum_{f \in \mathcal{F}} b_{nf} \quad (4a)$$

$$\text{s.t. } g^i \leq \sum_{(n_1, n_2) \in C(\mathcal{S})} c_{n_1, n_2}^i(\mathbf{b}, \mathbf{c}) \quad \forall i \in \mathcal{U}, \forall \mathcal{S} \subseteq \mathcal{V} \setminus \{t\} : s \in \mathcal{S} \quad (4b)$$

$$(3b), (3c), (3j), \quad b_{nf}, p_n, c_{nk} \in \{0, 1\}$$

$$g^i \in \{0, 1\} \quad \forall i \in \mathcal{U}. \quad (4c)$$

We refer to (4) as `BendersOCT-weighted`. The Benders cuts in (4b) are added dynamically through the Gurobi callback. We further observe that the separation algorithm of Aghaei et al. (2025) can be directly applied to identify violated cuts efficiently.

PROPOSITION 2. *Separation of the Benders cuts in (4b) follows the min-cut routine described in Algorithm 2 of Aghaei et al. (2025) (refer to Algorithm 3 in E-Companion).*

3. Imbalanced Datasets

In many real-world applications, the positive class is rare, and standard accuracy may be misleading. This section demonstrates that our framework accommodates both linear and nonlinear imbalance-aware objectives within a unified MIP architecture based on the `BendersOCT` structure. All objectives considered are functions of the confusion-matrix entries TP, TN, FP, FN. The proposed framework is distinguished by its modeling flexibility: any metric expressible as a function of these integer counts with a nonnegative denominator can be embedded within the MIP. Given a performance metric $h(\text{TP}, \text{TN}, \text{FP}, \text{FN})$, if h is nonlinear, we reformulate it using fractional programming, binary expansion, and McCormick envelopes. This yields a *unified* MIP model

applicable to a wide family of metrics—including F_β , MCC, balanced accuracy, G-Mean, Fowlkes–Mallows, and Jaccard/IoU—without altering the underlying structure.

We detail two representative nonlinear metrics: the F_β score (a linear-fractional measure) and the Matthews correlation coefficient (MCC, a correlation-type measure). Both are widely used in imbalanced classification. Formulations for other metrics (e.g., G-Mean, and Fowlkes–Mallows) follow the same pattern and appear in E-Companion EC.4.

We consider binary classification ($|\mathcal{K}| = 2$, labels $\{0, 1\}$). Let

$$n^+ = \sum_{i \in \mathcal{U}: y_i=1} w_i, \quad n^- = \sum_{i \in \mathcal{U}: y_i=0} w_i.$$

Then the confusion-matrix entries are

$$TP = \sum_{i \in \mathcal{U}: y_i=1} w_i g^i, \quad FN = n^+ - \sum_{i \in \mathcal{U}: y_i=1} w_i g^i, \quad (5)$$

$$TN = \sum_{i \in \mathcal{U}: y_i=0} w_i g^i, \quad FP = n^- - \sum_{i \in \mathcal{U}: y_i=0} w_i g^i. \quad (6)$$

3.1. F_β Score

The F_β score, including the widely adopted F1-score, is frequently used to evaluate binary classifiers when the dataset is imbalanced:

$$F_\beta = \frac{(1 + \beta^2) \text{Precision} \cdot \text{Recall}}{\beta^2 \text{Precision} + \text{Recall}} = \frac{(1 + \beta^2) \cdot TP}{\beta^2 n^+ + n^- + TP - TN}, \quad (7)$$

where TP and TN denote true positives and true negatives, respectively.

Recent optimal classification tree models have sought to directly maximize F1-score (Tu and Wu 2025, Tu et al. 2024, van der Linden et al. 2023, Demirović and Stuckey 2021, Lin et al. 2020), but their scalability remains limited. In our prior work (Tu and Wu 2025, Tu et al. 2024), we formulated the problem as a nonconvex MIQP, which becomes intractable for larger datasets or deeper trees. Here, we reformulate it as a pure MIP by linearizing the single bilinear term coupling F_β with confusion-matrix entries, thereby achieving substantial scalability gains (see Section 5.3.2).

Let $F_\beta \in [0, 1]$ be a decision variable representing the score. A direct MIQP formulation is:

$$\max F_\beta - \lambda \sum_{n \in \mathcal{B}} \sum_{f \in \mathcal{F}} b_{nf} \quad (8a)$$

$$\text{s.t. } F_\beta \cdot (\beta^2 n^+ + n^- + \text{TP} - \text{TN}) \leq (1 + \beta^2) \cdot \text{TP}, \quad (8b)$$

$$g^i \leq \sum_{(n_1, n_2) \in C(\mathcal{S})} c_{n_1, n_2}^i(\mathbf{b}, \mathbf{c}) \quad \forall i \in \mathcal{U}, \forall \mathcal{S} \subseteq \mathcal{V} \setminus \{t\} : s \in \mathcal{S}, \quad (8c)$$

$$(3b), (3c), (3j), \quad b_{nf}, p_n, c_{nk} \in \{0, 1\}, \quad (8d)$$

$$g^i \in \{0, 1\} \quad \forall i \in \mathcal{U}. \quad (8e)$$

The only nonlinearity appears in constraint (8b). Let $l = \lceil \log_2 |\mathcal{I}| \rceil$. Introduce binary variables δ_k for $k = 0, \dots, l$ and impose $n^- + \text{TP} - \text{TN} = \sum_{k=0}^l 2^k \delta_k$. Multiplying both sides by F_β yields $F_\beta(n^- + \text{TP} - \text{TN}) = \sum_{k=0}^l 2^k F_\beta \delta_k$. Introduce auxiliary variables γ_k for $k = 0, \dots, l$ such that $\gamma_k = F_\beta \delta_k$. Using McCormick envelopes (which are exact on $[0, 1] \times \{0, 1\}$), we impose $\gamma_k \leq \delta_k$, $\gamma_k \leq F_\beta$, $\gamma_k \geq F_\beta + \delta_k - 1$. The model (8) can thus be transformed into the following MIP model:

$$\max F_\beta - \lambda \sum_{n \in \mathcal{B}} \sum_{f \in \mathcal{F}} b_{nf} \quad (9a)$$

$$\text{s.t. } F_\beta(\beta^2 n^+ + n^-) + \sum_{k=0}^l 2^k \gamma_k \leq (1 + \beta^2) \sum_{i \in \mathcal{U}: y_i=1} w_i g^i, \quad (9b)$$

$$g^i \leq \sum_{(n_1, n_2) \in C(\mathcal{S})} c_{n_1, n_2}^i(\mathbf{b}, \mathbf{c}) \quad \forall i \in \mathcal{U}, \forall \mathcal{S} \subseteq \mathcal{V} \setminus \{t\} : s \in \mathcal{S}, \quad (9c)$$

$$(3b), (3c), (3j), \quad b_{nf}, p_n, c_{nk} \in \{0, 1\}, \quad (9d)$$

$$n^- + \text{TP} - \text{TN} = \sum_{k=0}^l 2^k \delta_k, \quad (9e)$$

$$\gamma_k \leq \delta_k, \quad \gamma_k \leq F_\beta, \quad \gamma_k \geq F_\beta + \delta_k - 1 \quad \forall k, \quad (9f)$$

$$g^i \in \{0, 1\} \quad \forall i \in \mathcal{U}. \quad (9g)$$

REMARK 1. The linearization introduces $l + 1 = \lceil \log_2 |\mathcal{I}| \rceil + 1$ new binary variables δ_k , the same number of continuous variables γ_k , and at most $3(l + 1)$ linear constraints from the McCormick

envelopes. Thus the additional model size is logarithmic in the number of (weighted) samples, and in practice the contribution of these variables and constraints is negligible compared to the structural variables (b, p, c, g) and the Benders cuts. This explains why the F_β formulation scales similarly to the accuracy-based model in our experiments.

3.2. Matthews Correlation Coefficient (MCC)

The Matthews correlation coefficient (MCC) is a correlation-based measure of classification quality that remains reliable under class imbalance:

$$\begin{aligned} \text{MCC} &= \frac{\text{TP} \cdot \text{TN} - \text{FP} \cdot \text{FN}}{\sqrt{(\text{TP} + \text{FP})(\text{TP} + \text{FN})(\text{TN} + \text{FP})(\text{TN} + \text{FN})}} \\ &= \frac{A}{\sqrt{n^+n^-UV}}, \end{aligned} \quad (10)$$

where we define

$$A = n^+TN + n^-TP - n^+n^-, \quad U = TP - TN + n^-, \quad V = TN - TP + n^+.$$

PROPOSITION 3. *For any binary dataset, maximizing the MCC is equivalent to maximizing the square of the MCC in the FlowOCT structure.*

Motivated by Proposition 3, we introduce a decision variable $\text{MCC2} \in [0, 1]$ representing MCC^2 and obtain the following non-convex MIQCP formulation for maximizing the MCC in the Benders-OCT structure:

$$\begin{aligned} &\max \text{MCC2} \\ \text{s.t.} \quad &n^+n^- \cdot \text{MCC2} \cdot S \leq A^2, \\ &A = n^+TN + n^-TP - n^+n^-, \\ &U = TP - TN + n^-, \quad V = TN - TP + n^+, \\ &S = UV, \\ &A \geq 0, \\ &0 \leq \text{MCC2} \leq 1, \\ &\text{Constraints (5)–(6), (8c)–(8e).} \end{aligned} \quad (11)$$

In model (11), the nonlinear terms $\text{MCC2} \cdot (UV)$ and A^2 make the model non-convex and hard to solve. We therefore linearize $\text{MCC2} \cdot (UV)$ and A^2 via binary expansions and McCormick envelopes.

(i) *Binary expansion of $U \cdot V$.* Since $0 \leq U, V \leq n^+ + n^- = |\mathcal{I}|$, we need at most $L = \lceil \log_2 |\mathcal{I}| \rceil$ binary digits to represent each of U and V . Introduce binary variables u_r, v_s for $r, s = 0, \dots, L$ and write

$$U = \sum_{r=0}^L 2^r u_r, \quad V = \sum_{s=0}^L 2^s v_s. \quad (12)$$

Then introduce binary variables χ_{rs} enforcing $\chi_{rs} = u_r \wedge v_s$, and obtain

$$UV = \sum_{r=0}^L \sum_{s=0}^L 2^{r+s} \chi_{rs}, \quad (13)$$

with constraints:

$$\chi_{rs} \leq u_r, \quad \chi_{rs} \leq v_s, \quad \chi_{rs} \geq u_r + v_s - 1 \quad \forall r, s. \quad (14)$$

(ii) *Linearization of $\text{MCC2} \cdot (UV)$.* Define $\theta_{rs} = \text{MCC2} \cdot \chi_{rs}$ and impose McCormick envelopes:

$$\theta_{rs} \leq \chi_{rs}, \quad \theta_{rs} \leq \text{MCC2}, \quad \theta_{rs} \geq \text{MCC2} - (1 - \chi_{rs}) \quad \forall r, s, \quad (15)$$

which implies

$$\text{MCC2}(UV) = \sum_{r=0}^L \sum_{s=0}^L 2^{r+s} \theta_{rs}. \quad (16)$$

(iii) *Linearize the quadratic term A^2 .* Since $|A| \leq n^+ n^-$, let $T = \lceil \log_2(n^+ n^-) \rceil$. Introduce binary variables $\beta_t \in \{0, 1\}$ for $t = 0, \dots, T$ such that

$$A = \sum_{t=0}^T 2^t \beta_t. \quad (17)$$

With “AND” binaries $\pi_{tt'} \in \{0, 1\}$ enforcing $\pi_{tt'} = \beta_t \wedge \beta_{t'}$, we obtain

$$A^2 = \sum_{t=0}^T \sum_{t'=0}^T 2^{t+t'} \pi_{tt'}, \quad (18)$$

with constraints:

$$\pi_{tt'} \leq \beta_t, \quad \pi_{tt'} \leq \beta_{t'}, \quad \pi_{tt'} \geq \beta_t + \beta_{t'} - 1 \quad \forall t, t'. \quad (19)$$

Replacing the nonlinear terms $\text{MCC2} \cdot (UV)$ and A^2 in model (11) with the linear expressions (16) and (18), we obtain the following MIP formulation:

$$\begin{aligned}
 & \max \text{MCC2} \\
 \text{s.t. } & n^+ n^- \sum_{r=0}^L \sum_{s=0}^L 2^{r+s} \theta_{rs} \leq \sum_{t=0}^T \sum_{t'=0}^T 2^{t+t'} \pi_{tt'}, \\
 & A = n^+ \text{TN} + n^- \text{TP} - n^+ n^-, \\
 & U = \text{TP} - \text{TN} + n^-, \quad V = \text{TN} - \text{TP} + n^+, \\
 & U = \sum_{r=0}^L 2^r u_r, \quad V = \sum_{s=0}^L 2^s v_s, \\
 & 0 \leq \text{MCC2} \leq 1, \quad A \geq 0, \\
 & \text{Constraints (5)–(6), (8c)–(8e), (14)–(15), (19).}
 \end{aligned} \tag{20}$$

REMARK 2. The MCC linearization adds $2(L+1) + (L+1)^2 + (T+1) + (T+1)^2$ binary variables and $3(L+1)^2 + 3(L+1)^2 + 3(T+1)^2$ linear constraints. Hence both the number of auxiliary 0–1 variables and the number of additional constraints grow polylogarithmically in the sample size $|\mathcal{I}|$. The constant factors are larger than for the F_β formulation, but for moderate-depth trees and UCI-scale datasets this overhead remains manageable and the resulting MIP is tractable. For very large training sets or substantially deeper trees, the MCC formulation can become heavy, and using lighter objectives such as F_β may be more practical.

3.3. Combinations

Following the same template as for the F_β score and MCC, we can derive MIQP and MIP formulations for any metric computed from the confusion table. Appendix EC.4 provides formulations for other commonly used performance metrics.

In binary classification, decision makers rarely choose a model based on a single performance indicator (e.g., accuracy or F1-score), because different metrics emphasize different trade-offs and may rank models inconsistently, especially under class imbalance. Instead, a practical strategy is to select a *stable* classifier that performs competitively across a set of metrics—such as F1-score, balanced accuracy (BA), and MCC. Our BendersOCT architecture makes it straightforward to maximize any convex combination of metrics constructed from the confusion matrix. For example, to maximize both accuracy and F_β , we consider the MIP model:

$$\max \quad \alpha_1 F_\beta + \frac{\alpha_2}{|\mathcal{I}|} \sum_{i \in \mathcal{U}} w_i g^i - \lambda \sum_{n \in \mathcal{B}} \sum_{f \in \mathcal{F}} b_{nf}, \tag{21a}$$

$$\text{s.t.} \quad \text{Constraints (9b)–(9g),} \tag{21b}$$

where $\alpha_1, \alpha_2 \geq 0$ control the relative importance of F_β and accuracy.

4. Acceleration Techniques

We now describe two complementary mechanisms that improve scalability of our formulations: (i) cutting-plane techniques based on conflict subsets and feature-activated inequalities; and (ii) a feasible-solution injection framework that combines depth-incremental warm starts with LP-guided heuristic injections at MIP nodes.

4.1. Cutting Planes

4.1.1. Valid inequalities We first exploit the fact that duplicated feature vectors with different labels cannot all be classified correctly by any decision tree.

DEFINITION 2 (CONFLICT SUBSET). A subset $\mathcal{G}_s \subseteq \mathcal{U}$ is a *conflict subset* if it contains instances with identical features but non-identical labels. For each class $k \in \mathcal{K}$, define $\mathcal{G}_{sk} = \{i \in \mathcal{G}_s : y_i = k\}$, so that $\mathcal{G}_s = \bigcup_{k \in \mathcal{K}} \mathcal{G}_{sk}$ and $|\mathcal{G}_s| = \sum_{k \in \mathcal{K}} |\mathcal{G}_{sk}|$.

If all points in \mathcal{G}_s share the same feature vector, any decision tree induces the same path and prediction for all of them. Hence at most one class in \mathcal{G}_s can be classified correctly.

THEOREM 1. *For any conflict subset \mathcal{G}_s , the following inequality is valid for BendersOCT-weighted:*

$$\sum_{i \in \mathcal{G}_s} g^i \leq \max_{k \in \mathcal{K}} |\mathcal{G}_{sk}|. \quad (22)$$

EXAMPLE 1. Consider the following example with $\mathcal{K} = \{0, 1\}$, four instances $\mathcal{U} = \{1, 2, 3, 4\}$, and four features $\mathcal{F} = \{1, 2, 3, 4\}$, with unit weights $w_i = 1$ and

$$\mathbf{x}_1 = (0, 1, 0, 0)^\top, \quad y_1 = 0; \quad \mathbf{x}_2 = (0, 1, 0, 0)^\top, \quad y_2 = 1;$$

$$\mathbf{x}_3 = (1, 0, 1, 0)^\top, \quad y_3 = 0; \quad \mathbf{x}_4 = (1, 0, 1, 1)^\top, \quad y_4 = 1.$$

Under the full feature set \mathcal{F} , the only conflict subset is $\mathcal{G}_1 = \{1, 2\}$. We have $\mathcal{G}_{10} = \{1\}$, $\mathcal{G}_{11} = \{2\}$, so $\max_k |\mathcal{G}_{1k}| = 1$ and

$$g^1 + g^2 \leq 1,$$

which encodes that instances 1 and 2 must share a prediction path and thus cannot both be correct.

The inequalities in Theorem 1 extend naturally to *feature-activated* conflicts that arise when a subset of features is disabled.

PROPOSITION 4 (Feature-activated conflict subset). *Let $\mathcal{F}' \subseteq \mathcal{F}$ and suppose that, when features in \mathcal{F}' are removed (i.e., the tree cannot branch on them), a collection of instances merges into a conflict subset $\mathcal{G}'_s \subseteq \mathcal{U}$. Partition \mathcal{G}'_s by class as $\mathcal{G}'_{sk} = \{i \in \mathcal{G}'_s : y_i = k\}$, $k \in \mathcal{K}$. Then the following inequality is valid for BendersOCT-weighted:*

$$\sum_{i \in \mathcal{G}'_s} g^i \leq \max_{k \in \mathcal{K}} |\mathcal{G}'_{sk}| + \left(|\mathcal{G}'_s| - \max_{k \in \mathcal{K}} |\mathcal{G}'_{sk}| \right) \sum_{n \in \mathcal{B}} \sum_{f \in \mathcal{F}'} b_{nf}. \quad (23)$$

Inequality (23) interpolates between two regimes: if $\sum_{n,f \in \mathcal{F}'} b_{nf} = 0$, the right-hand side reduces to $\max_k |\mathcal{G}'_{sk}|$, recovering the pure conflict bound; if $\sum_{n,f \in \mathcal{F}'} b_{nf} \geq 1$, the right-hand side becomes $|\mathcal{G}'_s|$, and the inequality is automatically satisfied. Thus, (23) prevents the LP relaxation from simultaneously (i) assigning $g^i \approx 1$ for all $i \in \mathcal{G}'_s$ and (ii) keeping features in \mathcal{F}' fractionally unused.

EXAMPLE 2. Reconsider Example 1 with $\mathcal{F}' = \{4\}$. In the reduced feature space $\{1, 2, 3\}$,

$$\mathbf{x}_3|_{\{1, 2, 3\}} = (1, 0, 1)^\top, \quad \mathbf{x}_4|_{\{1, 2, 3\}} = (1, 0, 1)^\top,$$

so instances 3 and 4 form a feature-activated conflict subset $\mathcal{G}'_1 = \{3, 4\}$ with $\mathcal{G}'_{10} = \{3\}$, $\mathcal{G}'_{11} = \{4\}$, $|\mathcal{G}'_1| = 2$, and $\max_k |\mathcal{G}'_{1k}| = 1$. Inequality (23) becomes

$$g^3 + g^4 \leq 1 + \sum_{n \in \mathcal{B}} b_{n4}.$$

If $\sum_n b_{n4} = 0$, at most one of $\{3, 4\}$ can be correct; if some split on feature 4 is used, the bound is ≥ 2 and the inequality is nonbinding.

4.1.2. Branch-and-cut implementation The number of pure conflict subsets \mathcal{G}_s is typically small, so the inequalities (22) are added as static constraints to the Benders master. In contrast, feature-activated conflict subsets \mathcal{G}'_s depend on the subset \mathcal{F}' of features that are effectively “switched off” in the LP relaxation and are separated dynamically.

Let $(\mathbf{b}^*, \mathbf{g}^*)$ be the LP solution at a given node. We observe empirically that most relaxations satisfy $g_i^* \approx 1$ for most $i \in \mathcal{U}$, and many features are essentially unused, that is, for most of the features $\sum_{n \in \mathcal{B}} b_{nf}^* \approx 0$. We therefore define

$$\mathcal{F}' = \left\{ f \in \mathcal{F} \mid \sum_{n \in \mathcal{B}} b_{nf}^* = 0 \right\},$$

group instances that share the same pattern on $\mathcal{F} \setminus \mathcal{F}'$ into subsets \mathcal{G}'_s , and check each for violation of (23). Whenever a violation is found, the corresponding cut is added via the solver’s callback function. These cuts depend only on (\mathbf{b}, \mathbf{g}) , and thus can be applied to Benders master (4) and all its variants (linear and nonlinear objectives). We refer to the resulting master with conflict and feature-activated cuts as BendersOCT-cut in our experiments.

4.2. Feasible-Solution Injection

From a branch-and-bound perspective, a strong initial incumbent immediately tightens the global upper bound, shrinks the portion of the search space that must be explored, and improves node selection and pruning efficiency (Morrison et al. 2016). Prior work has shown that injecting the CART solution can quickly produce a reasonable integer-feasible tree and reduce solution time (Tu and Wu 2025, Bertsimas and Dunn 2017). However, CART is a heuristic and its solution quality can be limited especially for deeper trees or nonlinear objectives. We therefore design a unified feasible-solution injection framework that enhances the scalability of `BendersOCT`. It relies on three empirical observations:

1. If the MIP only considers the features used by CART, then `BendersOCT` often improves on the CART objective at the same depth.
2. Optimal classification trees typically use only a few features (often ≤ 10), and shallow trees with small feature sets can be solved quickly.
3. Any shallow tree is a feasible subtree of deeper trees with the same branching pattern; thus, solutions at smaller depths can be lifted to provide warm starts for deeper models.

These observations motivate a three-layer strategy: (i) a depth-incremental warm start from depth 2; (ii) a global Random Forest (RF) ranking that guides the evolution of feature sets; and (iii) an LP-guided node heuristic that injects additional incumbents during the MIP search.

4.2.1. Depth-incremental warm start and RF-guided feature sets We solve a sequence of OCT problems for depths $d = 2, \dots, D$, using a single global RF ranking. Let T_d denote the depth- d tree and \mathcal{F}_d its feature set. The procedure is detailed Algorithm 1.

First, fit a CART of depth D and let $\mathcal{F}_{\text{CART}} = \{f \in \mathcal{F} \mid f \text{ is used in CART}\}$. Next, fit an RF and compute importance scores I_f for $f \in \mathcal{F}$, then obtain the global ranking $L = (f^{(1)}, f^{(2)}, \dots, f^{(p)})$ such that $I_{f^{(1)}} \geq I_{f^{(2)}} \geq \dots \geq I_{f^{(p)}}$.

For $d = 2$, we set $\mathcal{F}_2 \leftarrow \mathcal{F}_{\text{CART}} \cup \{\text{first } k \text{ indices in } L \setminus \mathcal{F}_{\text{CART}}\}$. We restrict the data to $X_{\mathcal{F}_2}$, solve the OCT MIP on $(X_{\mathcal{F}_2}, y)$ to obtain a warm start S_2^{warm} , and then solve the full depth-2 MIP on (X, y) with this warm start and node-level heuristics, yielding T_2 and an updated \mathcal{F}_2 .

For $d > 2$, we iterate $\mathcal{F}_d \leftarrow \mathcal{F}_{d-1} \cup \{\text{next } k \text{ indices in } L \setminus \mathcal{F}_{d-1}\}$, embed T_{d-1} into a depth- d topology over \mathcal{F}_d to form a reduced warm start S_d^{sub} , solve the reduced problem on $(X_{\mathcal{F}_d}, y)$ to obtain \tilde{T}_d , and lift \tilde{T}_d back to the full space to construct a full warm start S_d^{full} . The depth- d OCT MIP on (X, y) is then re-optimized with S_d^{full} and node-level heuristics to obtain T_d . This process yields a sequence (T_2, \dots, T_D) of structurally consistent warm starts with strong objective values.

Algorithm 1 FEASIBLESOLUTIONINJECTION for depth- D OCT (schematic)

Require: $X \in \mathbb{R}^{n \times p}$, y ; depth $D \geq 2$; RF ranking L ; feature increment k

```

1: Fit depth- $D$  CART;  $\mathcal{F}_{\text{CART}} \leftarrow$  features used
2: Fit RF; obtain ranking  $L = (f^{(1)}, \dots, f^{(p)})$ 
3: for  $d = 2, \dots, D$  do
4:   if  $d = 2$  then
5:      $\mathcal{F}_2 \leftarrow \mathcal{F}_{\text{CART}} \cup (\text{first } k \text{ in } L \setminus \mathcal{F}_{\text{CART}})$ 
6:     Solve OCT on  $(X_{\mathcal{F}_2}, y) \Rightarrow S_2^{\text{warm}}$ 
7:     Solve depth-2 OCT on  $(X, y)$  with  $S_2^{\text{warm}} \Rightarrow T_2$ 
8:   else
9:      $\mathcal{F}_d \leftarrow \mathcal{F}_{d-1} \cup (\text{next } k \text{ in } L \setminus \mathcal{F}_{d-1})$ 
10:    Embed  $T_{d-1}$  into depth- $d$  over  $\mathcal{F}_d \Rightarrow S_d^{\text{sub}}$ 
11:    Solve OCT on  $(X_{\mathcal{F}_d}, y)$  with  $S_d^{\text{sub}} \Rightarrow \tilde{T}_d$ 
12:    Lift  $\tilde{T}_d$  to full space  $\Rightarrow S_d^{\text{full}}$ 
13:    Solve depth- $d$  OCT on  $(X, y)$  with  $S_d^{\text{full}} \Rightarrow T_d$ 
14:   end if
15: end for
16: return  $T_D$ 
  
```

4.2.2. Heuristic injection at MIP nodes Within each MIP solve, we further accelerate convergence by injecting additional feasible solutions at the nodes of a branch-and-bound tree. The procedure is detailed Algorithm 2. Let $\mathbf{b}^* = (b_{nf}^*)$ be the LP-relaxation values of the branching variables at a node. Define the saliency score

$$\text{score}(f) = \sum_{n \in \mathcal{B}} b_{nf}^*, \quad f \in \mathcal{F},$$

and let $\mathcal{S}_{\text{inc}} \subseteq \mathcal{F}$ be the feature set of the incumbent tree. We form a candidate feature subset

$$\mathcal{S}_1 = \mathcal{S}_{\text{inc}} \cup \left\{ \text{top-3 } f \in \mathcal{F} \setminus \mathcal{S}_{\text{inc}} \text{ by } \text{score}(f) \right\}.$$

A history set \mathcal{H} stores previously tried subsets; if $\mathcal{S}_1 \in \mathcal{H}$, the attempt is skipped. Heuristic injections are scheduled only at selected nodes.

On \mathcal{S}_1 , we solve a short-horizon sub-MIP to obtain an integer tree, lift it to a full solution $(\mathbf{b}, \mathbf{p}, \mathbf{c}, \mathbf{g})$, and inject it via `cbSetSolution()` and `cbUseSolution()` whenever the objective improves the incumbent.

Algorithm 2 NODEHEURISTICINJECTION at a MIP node (schematic)

Require: LP solution \mathbf{b}^* ; incumbent feature set \mathcal{S}_{inc} ; history \mathcal{H}

```
1:  $\text{score}(f) \leftarrow \sum_{n \in \mathcal{B}} b_{nf}^*$  for all  $f \in \mathcal{F}$ 
2:  $\mathcal{S}_1 \leftarrow \mathcal{S}_{\text{inc}} \cup \{\text{top-3 } f \notin \mathcal{S}_{\text{inc}} \text{ by } \text{score}(f)\}$ 
3: if  $\mathcal{S}_1 \in \mathcal{H}$  then
4:   return
5: end if
6:  $\mathcal{H} \leftarrow \mathcal{H} \cup \{\mathcal{S}_1\}$ 
7: Solve sub-MIP on  $\mathcal{S}_1 \Rightarrow$  integer tree
8: Lift to full solution  $(\mathbf{b}, \mathbf{p}, \mathbf{c}, \mathbf{g})$ 
9: if objective improves incumbent then
10:   cbSetSolution(), cbUseSolution()
11: end if
```

5. Evaluation

In this section, we evaluate various versions of our model and conduct a comparative analysis with the current state-of-the-art approaches.

5.1. Experimental Setup

Datasets. We use 50 datasets compiled from prior work (Aghaei et al. 2025, Demirović et al. 2023), covering a wide range of sizes and class balances: 24 small datasets (fewer than 1,000 samples), 12 medium datasets (1,000–5,000 samples), and 12 large datasets (more than 5,000 samples). Detailed statistics are reported in Table EC.1. Following common practice, datasets containing categorical and/or continuous features are binarized via supervised discretization using the Minimum Description Length Principle (MDLP) (Fayyad and Irani 1993), followed by one-hot encoding. While alternative discretization strategies may improve downstream performance, a thorough investigation is left to future work.

Model training. For each dataset, we construct five independent random splits into training, validation, and test sets with proportions 50%/25%/25%, consistent with prior studies (Aghaei et al. 2025). All MIP models are solved using Gurobi 11.0 (Gurobi Optimization 2023). The binarized datasets are publicly available at <https://github.com/Tommytutu/Benders-cut>, and the source code will be released subsequently.

5.2. Comparison to State-of-the-Art Methods

In this section, we evaluate the scalability of BendersOCT-cut relative to state-of-the-art open-source baselines. The first is the MIP based formulation BendersOCT (Aghaei et al. 2025) which has shown to be more scalable than the previous MIP based models. The second is the DP based model, BendersOCT (Subramanian and Sun 2023) which is much more scalable than the existing MIP based models and can generalize to nonlinear classification metrics such as F1-score.

5.2.1. Comparing with BendersOCT We compare the BendersOCT baseline (Aghaei et al. 2025) with the following two variants show the efficiency of the cutting planes and instance reduction method:

- BendersOCT-weighted: the weighted master formulation in (4).
- BendersOCT-weighted-cut: BendersOCT-weighted solved with the branch and cut algorithm described in Section 4.1.2.

For fair comparison, we don't use any warm-start solutions for the MIP models (BendersOCT, BendersOCT-weighted and BendersOCT-weighted-cut). Set $\lambda = 0.01$ and runtime = 900 seconds, we train the MIP models on the training set and report the runtime, objective value and optimality gap. The optimality gap is defined as $\text{Gap} = 100 \times \frac{\text{UB} - \text{LB}}{\text{UB}} \%$, where UB is the best incumbent objective and LB is the global bound at termination. Figure 2 summarizes in-sample performance in terms of optimality gap, runtime, and objective values.

In Figure 2 (a), along the time axis, BendersOCT-weighted-cut solves the largest number of instances within the time limit, followed by BendersOCT-weighted, with BendersOCT being the slowest across all depths. Specifically, BendersOCT-weighted-cut solves 140 instances to optimality within 900s, BendersOCT-weighted solves 129 instances to optimality within 900s, BendersOCT solves 118 instances to optimality within 900s. BendersOCT-weighted-cut can solve 118 instances to optimality with less than 45 seconds, yielding more than a $\frac{900}{45} = 20\times$ speedup over BendersOCT. Along the gap axis, BendersOCT-weighted-cut consistently achieves smaller optimality gaps than both alternatives. As Figure 2 (b) shows, BendersOCT-weighted-cut can obtain better objective values as depth increases.

5.2.2. Comparison with `streeD` We compare our model with methods designed for optimizing nonlinear classification metrics. Lin et al. (2020) proposed a dynamic programming (DP) approach for objectives such as F1-score, but observed that the F1-score is harder to optimize since

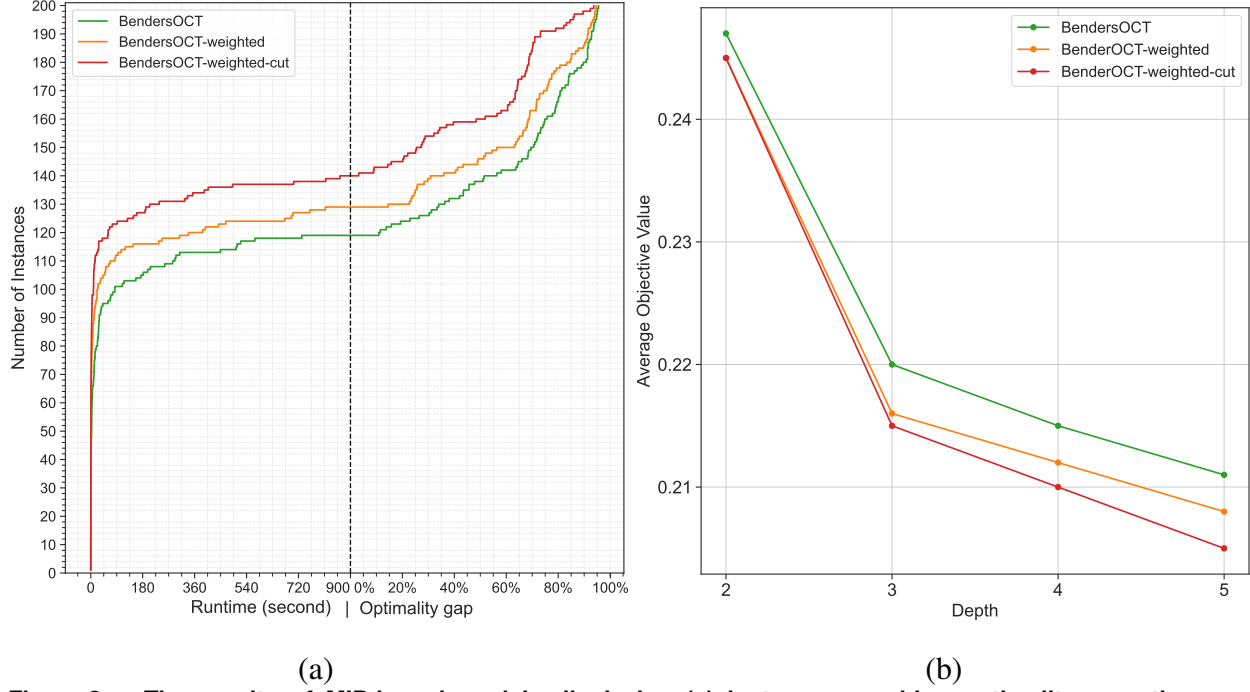


Figure 2 The results of MIP-based models displaying (a) instances reaching optimality over time and instances attaining a prescribed optimality-gap threshold at the time limit, (b) the average objective value by each approach across depths $d \in \{2,3,4,5\}$.

optimal label assignments in different leaves are interdependent. They introduced a heuristic parameter ω to simplify the problem, sacrificing optimality. Demirović and Stuckey (2021) developed a DP-based method capable of optimizing functions monotonic in both class misclassification scores (e.g., F1-score, Matthews correlation coefficient), but it lacks scalability—failing to find feasible solutions within one hour for many depth-4 instances (see Table 2 in their paper). van der Linden et al. (2023) improved scalability and proposed an anytime algorithm, *StreeD*. However, in their released implementation, only F1-score maximization is supported despite claims of generality to other nonlinear metrics. Therefore, we compare our BendersOCT-cut with *StreeD* on the task of maximizing F1-score. For a fair comparison, we set the model complexity parameter λ to a small value of 0.0001 for BendersOCT-cut. In addition, we fix the maximum number of branching nodes to $2^D - 1$ (`max_num_nodes = $2^D - 1$`), corresponding to a full binary tree of depth D .

We use the 18 binary datasets on which Demirović and Stuckey (2021) failed to find depth-4 solutions, setting a 90-second time limit. Performance is evaluated by in-sample F1-score and runtime (Table 1, best results in bold). At depth 4, BendersOCT-cut achieves the best F1-score on 6 datasets versus 3 for *StreeD*. At depth 5, BendersOCT-cut demonstrates superior scalability, achieving the best results on 11 datasets, while *StreeD* performs best on only 2 and fails to find

feasible solutions for 5 datasets. Notably, on the `appendicitis` dataset, BendersOCT-cut attains the optimal F1-score (0.889), whereas `StreeD` produces a suboptimal result (0.75).

Table 1 The in-sample F1-score and runtime (s) for maximizing F1-score by BendersOCT-cut and StreeD. If no feasible solution is found within 90 seconds, then denote with ‘—’. Best results are shown in bold.

instance	D=4				D=5			
	F1-score		Time		F1-score		Time	
	BendersOCT-cut	StreeD	BendersOCT-cut	StreeD	BendersOCT-cut	StreeD	BendersOCT-cut	StreeD
appendicitis	0.824	0.750	2.7	90.2	0.889	0.750	4.7	90.9
biodeg	0.875	0.875	91.3	90.9	0.875	0.883	90.9	90.9
cleve	0.931	0.866	91.8	90.9	0.937	0.866	90.3	90.7
colic	0.959	0.947	90.4	90.9	0.959	0.947	90.5	90.8
compas	0.689	0.689	91.2	28.7	0.689	0.689	90.2	90.5
diabetes	0.869	0.869	90.5	90.1	0.898	—	91.3	90.6
fico	0.721	0.721	91.0	90.9	0.730	—	93.0	91.0
german	0.874	0.874	90.5	91.0	0.894	0.874	90.5	90.9
heart	0.930	0.862	90.3	90.9	0.945	0.862	90.3	90.9
hepatitis	1.000	1.000	96.7	90.9	1.000	1.000	91.1	90.7
HTRU_2	0.876	0.892	90.5	90.8	0.902	—	90.5	90.4
hungarian	0.844	0.835	91.3	90.9	0.844	0.835	94.4	90.9
magic04	0.751	0.750	95.8	90.8	0.751	0.751	90.7	102.8
pendigits	0.999	0.999	97.6	90.8	0.999	1.000	91.0	90.5
promoters	1.000	1.000	11.8	52.5	1.000	1.000	14.2	90.6
spambase	0.889	0.889	95.4	90.3	0.889	—	90.4	90.7
vehicle	0.917	0.917	91.5	90.9	0.917	0.917	91.3	90.3
yeast	0.615	0.615	90.5	90.9	0.615	—	90.6	90.8

5.3. Ablation Study

5.3.1. Benefits of Feasible Solution Injections Table 2 compares the proposed feasible-solution injection strategy (Section 4.2) with a CART-based warm start, averaged over 50 datasets for depths $d = 2, \dots, 5$. *Injection Objval* reports the objective value of the initial incumbent produced by each warm-start strategy, while *Final Objval* and *Final Gap* correspond to the best objective value and MIP gap after 900 seconds of Gurobi runtime.

Across all depths, our method yields consistently better initial incumbents than the CART warm start (e.g., 0.239 vs. 0.262 at $d = 2$, 0.199 vs. 0.224 at $d = 5$), showing that the proposed warm-start method construct substantially stronger starting solutions. These advantages persist and even

amplify after full optimization: the final objective values under our warm start are uniformly lower than those under CART (e.g., 0.229 vs. 0.245 at $d = 2$, 0.195 vs. 0.202 at $d = 5$). Moreover, the average final gap is reduced by roughly 10–14 percentage points across depths (from 18.3% to 4.0% at $d = 2$, and from 35.6% to 26.3% at $d = 5$), indicating faster convergence and tighter bounds. Overall, the proposed feasible-solution injection framework substantially strengthens both the initial and final performance of the branch-and-cut procedure compared with a standard CART-based warm start.

Table 2 The comparative results of the two warm start strategies.

Depth	Injection Objval		Final Objval		Final Gap	
	This paper	CART	This paper	CART	This paper	CART
2	0.239	0.262	0.229	0.245	4.0%	18.3%
3	0.208	0.242	0.203	0.215	13.8%	28.4%
4	0.201	0.228	0.199	0.211	22.3%	33.3%
5	0.199	0.224	0.195	0.202	26.3%	35.6%

5.3.2. Benefits of Linearization In this section, we experiment with the two kinds of formulations (MIP and MIQP) of the optimal classification trees with maximizing different objectives. For limited space, we only report the results of maximizing F1-score and MCC with depth=5 as shown in Table 3, and the results on the other nonlinear objectives are similar to MCC.

For maximizing F1-score, both the MIP and MIQP formulations can solve 6 instances (out of 18 instances) to optimality within the timelimit (900 seconds) at the depth of 5, while the method proposed by Demirović and Stuckey (2021) cannot find a feasible solution within 1 hour for these datasets (refer to the Table 2 in Demirović and Stuckey (2021)). When compared with the two formulations for maximizing F1-score, the MIP formulation performs better than MIQP in terms of gap, time and objective value. This shows that the linearization can improve scalability. Therefore, we can infer that our MIP formulation for the F1-score is more scalable than the MIQP proposed by Tu and Wu (2025). Moreover, the same linearization techniques can also be applied to their MIQP model. For maximizing MCC, MIP formulation performs better than MIQP in terms of gap, time and objective value.

Table 3 Results of the Two Formulations for Maximizing F1-score and MCC with Depth =5.

Instance	F1-score						MCC					
	Gap		Time		ObjVal		Gap		Time		ObjVal	
	MIP	MIQP	MIP	MIQP	MIP	MIQP	MIP	MIQP	MIP	MIQP	MIP	MIQP
appendicitis	0	0	0.04	0.05	0.04	0.04	0.0%	0.0%	0.3	33.7	0.396	0.396
biodeg	74.10%	77.30%	900.5	901.3	0.289	0.299	88.1%	100.0%	903.2	900.3	0.554	0.554
cleve	0	0	183.65	316.07	0.092	0.092	75.3%	96.9%	901.6	900.4	0.397	0.408
colic	11.20%	12.60%	900.22	900.13	0.103	0.103	24.3%	71.5%	900.1	900.4	0.227	0.365
compas	0	0	0.77	0.49	0.367	0.367	0.0%	100.0%	6.5	900.3	0.922	0.957
diabetes	64.70%	61.90%	901.16	900.68	0.176	0.176	96.1%	100.0%	903.1	900.3	0.787	0.814
fico	37.50%	47.90%	901.22	901.02	0.317	0.353	75.8%	100.0%	901.8	900.5	0.911	0.911
german	55.90%	57.50%	900.53	900.38	0.176	0.176	96.6%	100.0%	901.2	900.4	0.879	0.909
heart	38.40%	50.20%	900.11	900.52	0.151	0.161	70.4%	97.4%	901.5	900.3	0.420	0.518
hepatitis	0	0	1.56	3.74	0.06	0.06	0.0%	0.0%	10.1	43.9	0.100	0.100
HTRU_2	23.90%	28.20%	900.64	900.73	0.169	0.203	0.0%	100.0%	2.8	900.7	0.304	0.503
hungarian	40.90%	42.00%	900.19	900.14	0.127	0.127	59.0%	93.7%	900.8	900.2	0.428	0.571
magic04	80.60%	80.90%	901.1	900.64	0.355	0.48	87.3%	91.9%	900.9	900.5	0.817	0.924
pendigits	0	0	556.35	769.29	0.076	0.076	55.1%	91.9%	901.7	900.5	0.114	0.124
promoters	0	0	0.14	0.17	0.04	0.04	0.0%	0.0%	1.0	4.8	0.070	0.070
spambase	88.20%	82.60%	903.76	900.88	0.185	0.179	95.2%	100.0%	901.1	900.7	0.434	0.460
vehicle	32.10%	38.30%	900.29	900.28	0.116	0.116	74.6%	99.9%	901.4	900.0	0.234	0.292
yeast	89.50%	92.00%	901	29116.63	0.431	0.453	96.6%	100.0%	901.8	900.5	0.894	0.894
average	35.82%	37.30%	660.98	660.95	0.182	0.195	55.3%	80.2%	652.3	754.9	0.494	0.543

5.3.3. Benefits on Nonlinear Objectives We examine whether directly optimizing nonlinear objectives (e.g., F1-score and MCC) yields better generalization on imbalanced datasets compared with accuracy maximization. Table 4 reports out-of-sample results for depth-5 optimal trees trained under three objectives: accuracy (obj = Acc), F1-score (obj = F1), and MCC (obj = MCC). For each dataset and evaluation metric (Accuracy, F1-score, MCC), the best result is highlighted in bold.

As shown in Table 4, models trained to maximize F1-score or MCC generalize well to the test sets. In terms of test *accuracy*, the MCC-based model performs best on 11 of 18 datasets (including ties), compared with 7 each for the accuracy- and F1-based models. For test *F1-score*, the F1- and MCC-based models achieve 8 and 9 best results, respectively, both outperforming the accuracy-based model on several imbalanced datasets (e.g., compas, yeast). For test *MCC*, the MCC-based model leads on 11 datasets, clearly dominating the accuracy-based model.

Averaged results confirm these trends. Optimizing F1-score or MCC increases the mean test F1 from 0.717 (accuracy objective) to 0.760 and 0.753, representing absolute gains of 4.3% and 3.6%. Optimizing MCC raises the mean test MCC from 0.551 to 0.575 (a 2.4% improvement) while slightly improving accuracy (0.808 → 0.811). Overall, optimizing nonlinear objectives enhances nonlinear performance metrics on imbalanced test sets while maintaining or modestly improving accuracy relative to accuracy-only training.

Table 4 Out-of-sample results of different objectives when depth =5.

instance	Accuracy			F1-score			MCC		
	obj=Acc	obj=F1	obj=MCC	obj=Acc	obj=F1	obj=MCC	obj=Acc	obj=F1	obj=MCC
appendicitis	1.000								
biodeg	0.795	0.795	0.822	0.679	0.679	0.734	0.529	0.529	0.601
cleve	0.789	0.816	0.789	0.714	0.788	0.714	0.567	0.626	0.567
colic	0.793	0.815	0.783	0.843	0.857	0.831	0.579	0.623	0.549
compas	0.658	0.594	0.672	0.581	0.651	0.617	0.303	0.254	0.333
diabetes	0.786	0.781	0.802	0.861	0.850	0.852	0.501	0.475	0.555
fico	0.700	0.698	0.698	0.641	0.681	0.681	0.402	0.277	0.277
german	0.740	0.740	0.684	0.846	0.851	0.683	0.123	0.000	0.114
heart	0.882	0.809	0.868	0.826	0.745	0.809	0.745	0.624	0.719
hepatitis	0.718	0.718	0.718	0.353	0.353	0.353	0.299	0.299	0.299
HTRU2	0.973	0.979	0.979	0.828	0.871	0.871	0.822	0.862	0.862
hungarian	0.770	0.784	0.797	0.638	0.692	0.706	0.531	0.547	0.579
magic04	0.727	0.727	0.727	0.666	0.666	0.666	0.457	0.457	0.457
pendigits	0.986	0.990	0.993	0.924	0.948	0.965	0.917	0.943	0.961
promoters	0.741	0.741	0.741	0.759	0.759	0.759	0.532	0.532	0.532
spambase	0.855	0.855	0.862	0.815	0.815	0.826	0.697	0.697	0.712
vehicle	0.920	0.953	0.958	0.847	0.911	0.920	0.793	0.879	0.892
yeast	0.709	0.704	0.704	0.085	0.563	0.563	0.126	0.349	0.349
average	0.808	0.805	0.811	0.717	0.760	0.753	0.551	0.554	0.575

6. Conclusion

We developed a general framework for learning optimal classification trees via mixed-integer programming. The approach (i) compresses the training data through an instance-reduction scheme that aggregates duplicate instances with weights; (ii) builds on the Benders decomposition of

Aghaei et al. (2025) and strengthens the master problem using conflict-subset and feature-activated cutting planes; and (iii) extends to nonlinear, imbalance-aware objectives (e.g., F_β and MCC) through exact mixed-integer linear reformulations. Empirically, the proposed acceleration mechanisms—including a tailored branch-and-cut algorithm, instance reduction, and warm-start strategies—yield substantial improvements in scalability relative to the state-of-the-art MIP formulation BendersOCT. For nonlinear objectives, the resulting MIP models scale markedly better than MIQP counterparts and the DP-based approach StreeD (van der Linden et al. 2023), and trees trained to directly optimize nonlinear metrics often generalize better on those metrics for imbalanced data.

Despite the substantial gains, several challenges remain. First, optimizing nonlinear objectives (e.g., F1-score and MCC) at larger depths can still be computationally demanding due to the interaction of multiple count products and data-dependent binary variables. Second, performance depends on the quality of binarization; supervised discretization is convenient but may not be optimal for a given metric. Third, while our unique-instance reduction controls instance count, feature dimensionality still drives problem size. Future work will focus on more scalable linearization techniques and stronger convex-hull formulations for nonlinear objectives. In addition, given the strong dependence of scalability on the number of features, we plan to explore effective feature-selection strategies specifically tailored to our formulation.

References

- Aghaei S, Gómez A, Vayanos P (2025) Strong optimal classification trees. *Operations Research* 73(4):2223–2241.
- Alston B, Validi H, Hicks IV (2022) Mixed integer linear optimization formulations for learning optimal binary classification trees. *arXiv preprint arXiv:2206.04857* .
- Bertsimas D, Dunn J (2017) Optimal classification trees. *Machine Learning* 106(7):1039–1082.
- Bertsimas D, Dunn J, Paskov I (2022) Stable classification. *Journal of Machine Learning Research* 23(1):13401–13453.
- Bertsimas D, Dunn J, Pawlowski C, Zhuo YD (2019) Robust classification. *INFORMS Journal on Optimization* 1(1):2–34.
- Breiman L, Friedman J, Olshen R, Stone C (1984) *Classification and regression trees* (Monterey, CA: Wadsworth and Brooks).
- Chicco D, Jurman G (2020) The advantages of the matthews correlation coefficient (mcc) over f1 score and accuracy in binary classification evaluation. *BMC Genomics* 21(1):6.
- Demirović E, Hebrard E, Jean L (2023) Blossom: an anytime algorithm for computing optimal decision trees. *International Conference on Machine Learning*, 7533–7562 (PMLR).
- Demirović E, Lukina A, Hebrard E, Chan J, Bailey J, Leckie C, Ramamohanarao K, Stuckey PJ (2022) Murtree: Optimal decision trees via dynamic programming and search. *Journal of Machine Learning Research* 23(26):1–47.

- Demirović E, Stuckey PJ (2021) Optimal decision trees for nonlinear metrics. *Proceedings of the AAAI conference on Artificial Intelligence*, volume 35, 3733–3741.
- Fayyad UM, Irani KB (1993) Multi-interval discretization of continuous-valued attributes for classification learning. *International Joint Conference on Artificial Intelligence*, volume 93, 1022–1029.
- Firat M, Crognier G, Gabor AF, Hurkens CA, Zhang Y (2020) Column generation based heuristic for learning classification trees. *Computers & Operations Research* 116:104866.
- Günlük O, Kalagnanam J, Li M, Menickelly M, Scheinberg K (2021) Optimal decision trees for categorical data via integer programming. *Journal of Global Optimization* 81:233–260.
- Gurobi Optimization L (2023) Gurobi optimizer reference manual <Https://www.gurobi.com/solutions/gurobi-optimizer>.
- Laurent H, Rivest RL (1976) Constructing optimal binary decision trees is np-complete. *Information Processing Letters* 5(1):15–17.
- Lin J, Zhong C, Hu D, Rudin C, Seltzer M (2020) Generalized and scalable optimal sparse decision trees. *International Conference on Machine Learning*, 6150–6160 (PMLR).
- Mazumder R, Meng X, Wang H (2022) Quant-BnB: A scalable branch-and-bound method for optimal decision trees with continuous features. *International Conference on Machine Learning*, 15255–15277.
- Michini C, Zhou Z (2025) A polyhedral study of multivariate decision trees. *INFORMS Journal on Optimization* 7(1):61–82.
- Morrison DR, Jacobson SH, Sauppe JJ, Sewell EC (2016) Branch-and-bound algorithms: A survey of recent advances in searching, branching, and pruning. *Discrete Optimization* 19:79–102.
- Narodytska N, Ignatiev A, Pereira F, Marques-Silva J (2018) Learning optimal decision trees with SAT. *International Joint Conference on Artificial Intelligence 2018*, 1362–1368.
- Patel KK, Desaulniers G, Lodi A (2024) An improved column-generation-based matheuristic for learning classification trees. *Computers & Operations Research* 165:106579.
- Shati P, Cohen E, McIlraith SA (2023) Sat-based optimal classification trees for non-binary data. *Constraints* 28(2):166–202.
- Subramanian S, Sun W (2023) Scalable optimal multiway-split decision trees with constraints. *Proceedings of the AAAI Conference on Artificial Intelligence*, volume 37, 9891–9899.
- Tu J, Fan W, Wu Z (2024) Booleanoict: Optimal classification trees based on multivariate boolean rules. *arXiv preprint arXiv:2401.16133*.
- Tu J, Wu Z (2025) Inherently interpretable machine learning for credit scoring: Optimal classification tree with hyperplane splits. *European Journal of Operational Research* 322(2):647–664.
- van der Linden J, de Weerdt M, Demirović E (2023) Necessary and sufficient conditions for optimal decision trees using dynamic programming. *Advances in Neural Information Processing Systems* 36:9173–9212.
- Van Vlasselaer V, Eliassi-Rad T, Akoglu L, Snoeck M, Baesens B (2017) Gotcha! network-based fraud detection for social security fraud. *Management Science* 63(9):3090–3110.
- Verwer S, Zhang Y (2019) Learning optimal classification trees using a binary linear program formulation. *Proceedings of the AAAI Conference on Artificial Intelligence*, volume 33, 1625–1632.

E-Companion

EC.1. FlowOCT

In this section, we provide a simplified version of the formulation of

$$\text{maximize } (1 - \lambda) \sum_{i \in \mathcal{I}} \sum_{n \in \mathcal{B} \cup \mathcal{L}} z_{n,t}^i - \lambda \sum_{n \in \mathcal{V}} \sum_{f \in \mathcal{F}} b_{nf} \quad (\text{EC.1a})$$

$$\text{subject to } \sum_{f \in \mathcal{F}} b_{nf} + p_n + \sum_{m \in \mathcal{P}(n)} p_m = 1 \quad \forall n \in \mathcal{B} \quad (\text{EC.1b})$$

$$p_n + \sum_{m \in \mathcal{P}(n)} p_m = 1 \quad \forall n \in \mathcal{T} \quad (\text{EC.1c})$$

$$z_{a(n),n}^i = z_{n,\ell(n)}^i + z_{n,r(n)}^i + z_{n,t}^i \quad \forall n \in \mathcal{B}, i \in \mathcal{I} \quad (\text{EC.1d})$$

$$z_{a(n),n}^i = z_{n,t}^i \quad \forall n \in \mathcal{B} \cup \mathcal{L}, i \in \mathcal{I} \quad (\text{EC.1e})$$

$$z_{s,1}^i \leq 1 \quad \forall i \in \mathcal{I} \quad (\text{EC.1f})$$

$$z_{n,\ell(n)}^i \leq \sum_{f \in \mathcal{F}: x_f^i = 0} b_{nf} \quad \forall n \in \mathcal{B}, i \in \mathcal{I} \quad (\text{EC.1g})$$

$$z_{n,r(n)}^i \leq \sum_{f \in \mathcal{F}: x_f^i = 1} b_{nf} \quad \forall n \in \mathcal{B}, i \in \mathcal{I} \quad (\text{EC.1h})$$

$$z_{n,t}^i \leq c_{ny^i} \quad \forall n \in \mathcal{B} \cup \mathcal{L}, i \in \mathcal{I} \quad (\text{EC.1i})$$

$$\sum_{k \in \mathcal{K}} c_{nk} = p_n \quad \forall n \in \mathcal{B} \cup \mathcal{T} \quad (\text{EC.1j})$$

$$c_{nk} \in \{0, 1\} \quad \forall n \in \mathcal{B} \cup \mathcal{L}, k \in \mathcal{K} \quad (\text{EC.1k})$$

$$b_{nf} \in \{0, 1\} \quad \forall n \in \mathcal{B}, f \in \mathcal{F} \quad (\text{EC.1l})$$

$$p_n \in \{0, 1\} \quad \forall n \in \mathcal{B} \cup \mathcal{L} \quad (\text{EC.1m})$$

$$z_{a(n),n}^i, z_{n,t}^i \in \{0, 1\} \quad \forall n \in \mathcal{B} \cup \mathcal{L}, i \in \mathcal{I}, \quad (\text{EC.1n})$$

where $\lambda \in [0, 1]$ is a regularization parameter. An explanation of the constraints is as follows. Constraints (EC.1b) imply that at any node $n \in \mathcal{B}$ we either branch on a feature f (if $\sum_{f \in \mathcal{F}} b_{nf} = 1$), predict a label (if $p_n = 1$), or get pruned if a prediction is made at one of the node ancestors (i.e., if $\sum_{m \in \mathcal{P}(n)} p_m = 1$). Similarly constraints (EC.1c) ensure that any node $n \in \mathcal{B} \cup \mathcal{L}$ is either a

leaf node of the tree or is pruned. Constraints (EC.1d) are flow conservation constraints for each datapoint i and node $n \in \mathcal{B}$: they ensure that if a datapoint arrives at a node, then it must also leave the node through one of its descendants. Similarly, constraints (EC.1e) enforce flow conservation for each node $n \in \mathcal{L}$. The inequality constraints (EC.1f) imply that at most one unit of flow can enter the graph through the source for each datapoint. Constraints (EC.1g) (resp. (EC.1h)) ensure that if the flow of a datapoint is routed to the left (resp. right) at node n , then one of the features such that $x_f^i = 0$ (resp. $x_f^i = 1$) must have been selected for branching at the node. Constraints (EC.1i) guarantee that datapoints whose flow is routed to the sink node t are correctly classified. Constraints (EC.1j) make sure that each leaf node is assigned a predicted class $k \in \mathcal{K}$. The objective (EC.1a) maximizes the total number of correctly classified datapoints.

EC.2. Proof

EC.2.1. Proof of Proposition 1

Map each unique instance $i \in \mathcal{U}$ to the w_i duplicates in \mathcal{I} . Any feasible FlowOCT solution (b, p, c, z) on \mathcal{I} induces a feasible WFlowOCT solution by setting the same (b, p, c) and defining $z_{\cdot, \cdot}^i$ equal to the (common) flow pattern taken by its duplicates; then $\sum_n w_i z_{n,t}^i$ equals the total correct flow over all duplicates, so the objective values match (the regularization term is identical). Conversely, replicate each unique instance i exactly w_i times to expand (\mathcal{U}, w) back to \mathcal{I} ; any feasible WFlowOCT solution lifts to a feasible FlowOCT solution with the same (b, p, c) and duplicated flows, again preserving the objective. Optimality is preserved in both directions.

EC.2.2. Proof of Proposition 2

Fix an incumbent solution $(\bar{b}, \bar{c}, \bar{p}, \bar{g})$ of (4). For any instance $i \in \mathcal{U}$, consider the instance-specific capacity graph $G^i(\bar{b}, \bar{c})$ on $\mathcal{V} = \{s\} \cup \mathcal{B} \cup \mathcal{L} \cup \{t\}$ with arc capacities

$$\text{cap}(s, 1) = 1, \quad \text{cap}(n, \ell(n)) = \sum_{f: x_f^i = 0} \bar{b}_{nf}, \quad \text{cap}(n, r(n)) = \sum_{f: x_f^i = 1} \bar{b}_{nf}, \quad \text{cap}(n, t) = \bar{c}_{n,y_i},$$

and zero elsewhere. Let

$$\kappa_i = \min_{\mathcal{S} \subseteq \mathcal{V} \setminus \{t\}: s \in \mathcal{S}} \sum_{(n_1, n_2) \in C(\mathcal{S})} \text{cap}(n_1, n_2) \quad \text{and} \quad \mathcal{S}_i^* \in \arg \min(\cdot)$$

be the $s-t$ min-cut value and an associated minimizer. Then the most violated inequality among the Benders cuts (8c) for instance i is

$$g^i \leq \sum_{(n_1, n_2) \in C(\mathcal{S}_i^*)} c_{n_1, n_2}^i(\mathbf{b}, \mathbf{c}),$$

and a violation occurs if and only if $\bar{g}^i > \kappa_i$. Consequently, separation of (8c) reduces to computing an s - t min-cut on $G^i(\bar{\mathbf{b}}, \bar{\mathbf{c}})$ (as in Algorithm 2 of Aghaei et al. (2025)), which can be done in polynomial time.

For fixed $(\bar{\mathbf{b}}, \bar{\mathbf{c}}, \bar{\mathbf{p}})$, the sub problem for instance i is a maximum s - t flow on $G^i(\bar{\mathbf{b}}, \bar{\mathbf{c}})$. By the max-flow/min-cut theorem, every s - t cut \mathcal{S} yields a valid upper bound $g^i \leq \sum_{(n_1, n_2) \in C(\mathcal{S})} \text{cap}(n_1, n_2)$, and the tightest bound equals the min-cut value κ_i . Therefore, the most violated inequality for i is obtained from \mathcal{S}_i^* ; it is violated exactly when $\bar{g}^i > \kappa_i$. Standard max-flow algorithms (e.g., push–relabel or Dinic) compute κ_i and a minimizing cut in polynomial time, which provides a strong separation oracle for (8c).

EC.3. Separation procedure

Algorithm 3 Separation procedure for constraints (4b)

Input: $(\mathbf{b}, \mathbf{c}, \mathbf{p}, \mathbf{g}) \in \{0, 1\}^{\mathcal{B} \cdot \mathcal{F}} \cdot \{0, 1\}^{\mathcal{V} \cdot \mathcal{K}} \cdot \{0, 1\}^{\mathcal{V}} \cdot \mathbb{R}^{\mathcal{U}}$ satisfying (3b), (3c), (3j);

$i \in \mathcal{U}$: datapoint used to generate the cut.

Output: -1 if all constraints (4b) corresponding to i are satisfied;

source set \mathcal{S} of min-cut otherwise.

```

1: if  $g^i = 0$  then return  $-1$ 
2: Initialize  $n \leftarrow 1$  ▷ Current node = root
3: Initialize  $\mathcal{S} \leftarrow \{s\}$  ▷  $\mathcal{S}$  is in the source set of the cut
4: while  $p_n = 0$  do
5:    $\mathcal{S} \leftarrow \mathcal{S} \cup \{n\}$ 
6:   if  $c_{n, \ell(n)}^i(\mathbf{b}, \mathbf{w}) = 1$  then
7:      $n \leftarrow \ell(n)$  ▷ Datapoint  $i$  is routed left
8:   else if  $c_{n, r(n)}^i(\mathbf{b}, \mathbf{c}) = 1$  then
9:      $n \leftarrow r(n)$  ▷ Datapoint  $i$  is routed right
10:  end if
11: end while ▷ At this point,  $n$  is a leaf node of the tree
12:  $\mathcal{S} \leftarrow \mathcal{S} \cup \{n\}$ 
13: if  $g^i > c_{n, t}^i(\mathbf{b}, \mathbf{c})$  then ▷ Minimum cut  $\mathcal{S}$  with capacity 0 found
14:   return  $\mathcal{S}$ 
15: else ▷ Minimum cut  $\mathcal{S}$  has capacity 1, constraints (4b) are satisfied
16:   return  $-1$ 
17: end if

```

EC.3.1. Proof of Proposition 3

The sign of MCC depends on A . We show that there always exists a feasible solution with $A \geq 0$, i.e., $\text{MCC} \geq 0$. If we classify all examples as negative, then $\text{TP} = 0$ and $\text{TN} = n^-$, so

$$A = n^+n^- + n^- \cdot 0 - n^+n^- = 0.$$

Thus there exists a feasible solution with $\text{MCC} = 0$, and maximizing MCC is equivalent to maximizing MCC². \square

EC.3.2. Proof of Theorem 1

No single leaf can correctly assign different labels to instances with identical \mathbf{x} . At most one label k can be correctly assigned for all instances in \mathcal{G}_s , hence the bound (22).

EC.3.3. Proof of Proposition 4

For $i \in \mathcal{G}'_s$, let $\mathbf{x}_i|_{\mathcal{F} \setminus \mathcal{F}'}$ denote the projection of \mathbf{x}_i onto the coordinates in $\mathcal{F} \setminus \mathcal{F}'$. By assumption, removing \mathcal{F}' merges the involved unique instances into a conflict subset, hence

$$\mathbf{x}_i|_{\mathcal{F} \setminus \mathcal{F}'} = \mathbf{x}_j|_{\mathcal{F} \setminus \mathcal{F}'} \quad \text{for all } i, j \in \mathcal{G}'_s,$$

while their labels are not all identical. We analyze two cases.

Case 1: $\sum_{n \in \mathcal{B}} \sum_{f \in \mathcal{F}'} b_{nf} = 0$. No split in the tree uses a feature from \mathcal{F}' , so the routing of any sample depends only on $\mathbf{x}|_{\mathcal{F} \setminus \mathcal{F}'}$. Because all items in \mathcal{G}'_s have identical projections on these features, they follow the *same* path and reach the *same* leaf ℓ . Leaf ℓ predicts a single class $\hat{k} \in \mathcal{K}$; therefore, among the items in \mathcal{G}'_s the number correctly classified equals $|\mathcal{G}'_{s\hat{k}}|$, and

$$\sum_{i \in \mathcal{G}'_s} g^i = |\mathcal{G}'_{s\hat{k}}| \leq \max_{k \in \mathcal{K}} |\mathcal{G}'_{sk}|.$$

This is precisely the (tight) conflict bound that holds when the distinguishing features are unavailable.

Case 2: $\sum_{n \in \mathcal{B}} \sum_{f \in \mathcal{F}'} b_{nf} \geq 1$. In this case the right-hand side of (23) satisfies

$$\max_k |\mathcal{G}'_{sk}| + \left(|\mathcal{G}'_s| - \max_k |\mathcal{G}'_{sk}| \right) \sum_{n, f \in \mathcal{F}'} b_{nf} \geq \max_k |\mathcal{G}'_{sk}| + \left(|\mathcal{G}'_s| - \max_k |\mathcal{G}'_{sk}| \right) \cdot 1 = |\mathcal{G}'_s|.$$

Since $g^i \in \{0, 1\}$, we always have $\sum_{i \in \mathcal{G}'_s} g^i \leq |\mathcal{G}'_s|$. Hence the inequality (23) holds trivially in this case.

Combining the two cases proves (23) for all feasible (g^i, b_{nf}) .

Table EC.1 The number of unique samples for the 50 datasets.

dataset	$ \mathcal{F} $	$ \mathcal{K} $	$ \mathcal{I} $	$ \mathcal{U} $	dataset	$ \mathcal{F} $	$ \mathcal{K} $	$ \mathcal{I} $	$ \mathcal{U} $	
soybean	45	4	47	47	tic	958	27	2	958	958
appendicitis	530	2	106	106	german-credit	1000	112	2	1000	998
promoters	334	2	106	106	MaternalHealth	1014	23	3	1014	163
monk3	15	2	122	122	biodeg	1055	81	2	1055	931
monk1	15	2	124	124	messidor	1151	24	2	1151	231
hayes	15	3	132	78	banknote	1372	16	2	1372	52
iris	12	3	150	24	contraceptive	1473	21	3	1473	531
hepatitis	361	2	155	155	yeast	1484	89	2	1484	1423
monk2	15	2	169	169	car	1728	19	4	1728	1327
wine	32	3	178	128	wireless	2000	42	4	2000	1199
spect	22	2	267	228	kr	3196	65	2	3196	3173
heart	381	2	270	270	students	4424	96	3	4424	4267
breast	36	2	277	263	spambase	4601	132	2	4601	3594
hungarian	330	2	294	293	compas	6907	12	2	6907	213
cleve	395	2	303	302	pendigits	7494	216	2	7494	7415
column_3c	15	3	310	80	avila	10430	128	12	10430	8017
Ionosphere	143	2	351	316	fico	10459	17	2	10459	3243
derm	131	6	358	358	shuttleM	14500	198	2	14500	12978
dermatology	66	6	358	306	eeg	14980	61	2	14980	5933
colic	415	2	368	357	HTRU_2	17898	53	2	17898	2234
balance	20	3	625	625	magic04	19020	79	2	19020	10167
diabetes	112	2	768	768	default_credit	30000	44	4	30000	18239
IndiansDiabetes	11	2	768	175	Adult	32561	81	2	32561	23874
anneal	84	2	812	489	sepsis	110204	14	2	110204	140
vehicle	252	2	846	846	skin	245057	80	2	245057	5466

EC.4. Additional Metrics and Exact MIP Reformulations

This appendix collects mixed-integer formulations for three additional performance metrics that are frequently used on imbalanced datasets: linear objectives (balanced accuracy and class cost-sensitive loss) and the nonlinear objectives (Geometric Mean, Fowlkes–Mallows index, and the Jaccard/Intersection-over-Union (IoU)).

EC.4.1. Linear Metrics

We collect four commonly used *linear* objectives that are directly compatible with the formulation (4). In all cases, one may optionally add a structural penalty (e.g., complexity) $-\lambda \sum_{n \in \mathcal{B}} \sum_{f \in \mathcal{F}} b_{nf}$

to the objective without affecting linearity. The structural/tree constraints (flow, split selection, leaf assignment, Benders cuts) are assumed given by Eqs. (8c)–(8e).

Balanced Accuracy. Balanced Accuracy (BA) averages per-class recalls:

$$\text{BA} = \frac{1}{2} \left(\frac{\text{TP}}{n^+} + \frac{\text{TN}}{n^-} \right) = \frac{1}{2} \left(\frac{\sum_{i \in \mathcal{U}: y_i=1} w_i g^i}{n^+} + \frac{\sum_{i \in \mathcal{U}: y_i=0} w_i g^i}{n^-} \right). \quad (\text{EC.2})$$

Because n^+, n^- are data constants, maximizing BA is linear. Maximizing BA can be achieved by replacing the objective function of Problem (4) with

$$\max \quad \frac{1}{2} \left(\frac{\sum_{i \in \mathcal{U}: y_i=1} w_i g^i}{n^+} + \frac{\sum_{i \in \mathcal{U}: y_i=0} w_i g^i}{n^-} \right) - \lambda \sum_{n \in \mathcal{B}} \sum_{f \in \mathcal{F}} b_{nf}. \quad (\text{EC.3})$$

Class Cost-Sensitive Loss. Given misclassification costs $c^+ \geq 0$ for false negatives and $c^- \geq 0$ for false positives, the total cost is

$$\text{CS} = c^+ \text{FN} + c^- \text{FP} = c^+ \left(n^+ - \sum_{i \in \mathcal{U}: y_i=1} w_i g^i \right) + c^- \left(n^- - \sum_{i \in \mathcal{U}: y_i=0} w_i g^i \right). \quad (\text{EC.4})$$

A linear minimization (or, equivalently, maximization of a linear reward) is

$$\min \quad \text{CS} + \lambda \sum_{n,f} b_{nf} \iff \max \quad c^+ \text{TP} + c^- \text{TN} - \lambda \sum_{n \in \mathcal{B}} \sum_{f \in \mathcal{F}} b_{nf}. \quad (\text{EC.5})$$

Instance Cost-Sensitive Loss (minimize). Let $\kappa_i \geq 0$ be an instance-specific penalty for misclassifying i . The instance-level cost is

$$\text{ICS} = \sum_{i \in \mathcal{U}} \kappa_i w_i (1 - g^i) = \left(\sum_{i \in \mathcal{U}} \kappa_i w_i \right) - \sum_{i \in \mathcal{U}} \kappa_i w_i g^i,$$

so minimizing ICS is equivalent to maximizing the linear reward $\sum_i \kappa_i w_i g^i$. The corresponding linear program is

$$\min \quad \sum_{i \in \mathcal{U}} \kappa_i w_i (1 - g^i) + \lambda \sum_{n \in \mathcal{B}} \sum_{f \in \mathcal{F}} b_{nf} \iff \max \quad \sum_{i \in \mathcal{U}} \kappa_i w_i g^i - \lambda \sum_{n \in \mathcal{B}} \sum_{f \in \mathcal{F}} b_{nf}. \quad (\text{EC.6})$$

EC.4.2. Squared Geometric Mean (G-Mean²)

The G-Mean is defined as

$$\text{G-Mean} = \sqrt{\frac{\text{TP}}{\text{TP} + \text{FN}} \cdot \frac{\text{TN}}{\text{TN} + \text{FP}}} = \sqrt{\frac{\text{TP} \cdot \text{TN}}{n^+ n^-}},$$

so it suffices to maximize $\text{G2} = \text{G-Mean}^2 \in [0, 1]$:

$$\begin{aligned} \max \quad & \text{G2} - \lambda \sum_{n \in \mathcal{B}} \sum_{f \in \mathcal{F}} b_{nf} \\ \text{s.t.} \quad & \text{G2} \cdot (n^+ n^-) \leq \text{TP} \cdot \text{TN}, \\ & \text{Constraints (5)–(6), (8c)–(8e).} \end{aligned} \quad (\text{EC.7})$$

Let

$$\sum_{i \in \mathcal{U}: y_i=1} w_i g^i = \sum_{k=0}^p 2^k \gamma_k^+, \quad \sum_{i \in \mathcal{U}: y_i=0} w_i g^i = \sum_{l=0}^q 2^l \gamma_l^-. \quad (\text{EC.8})$$

We use the following AND binaries throughout:

$$\begin{aligned} \eta_{kl} = \gamma_k^+ \wedge \gamma_l^- & \Rightarrow \begin{cases} \eta_{kl} \leq \gamma_k^+, \eta_{kl} \leq \gamma_l^-, \\ \eta_{kl} \geq \gamma_k^+ + \gamma_l^- - 1, \end{cases} \\ \xi_{rs}^{++} = \gamma_r^+ \wedge \gamma_s^+ & \Rightarrow \begin{cases} \xi_{rs}^{++} \leq \gamma_r^+, \xi_{rs}^{++} \leq \gamma_s^+, \\ \xi_{rs}^{++} \geq \gamma_r^+ + \gamma_s^+ - 1, \end{cases} \end{aligned}$$

so that

$$\text{TP} \cdot \text{TN} = \sum_{k=0}^p \sum_{l=0}^q 2^{k+l} \eta_{kl}, \quad \text{TP}^2 = \sum_{r=0}^p \sum_{s=0}^q 2^{r+s} \xi_{rs}^{++}.$$

Substitute the binary expansions of TP and TN and linearize $\gamma_k^+ \gamma_l^-$ with η_{kl} . Model (EC.7) is equivalent to the following MIP:

$$\begin{aligned} \max \quad & \text{G2} - \lambda \sum_{n \in \mathcal{B}} \sum_{f \in \mathcal{F}} b_{nf} \\ \text{s.t.} \quad & \text{G2} \cdot (n^+ n^-) \leq \sum_{k=0}^p \sum_{l=0}^q 2^{k+l} \eta_{kl} \\ & \eta_{kl} \leq \gamma_k^+, \eta_{kl} \leq \gamma_l^-, \eta_{kl} \geq \gamma_k^+ + \gamma_l^- - 1 \quad \forall k, l, \\ & (\text{EC.8}) \text{ and (8c)–(8e).} \end{aligned} \quad (\text{EC.9})$$

EC.4.3. Fowlkes–Mallows (squared)

The Fowlkes–Mallows index is

$$FM = \sqrt{\frac{TP}{TP+FP} \cdot \frac{TP}{TP+FN}} = \sqrt{\frac{TP^2}{n^+ (n^- + TP - TN)}}.$$

Maximizing FM is equivalent to maximizing $FM2 := FM^2 \in [0, 1]$.

MIQCP.

$$\begin{aligned} & \max FM2 \\ \text{s.t. } & FM2 \cdot [n^+ (n^- + TP - TN)] \leq TP^2, \\ & \text{Constraints (5)–(6), (8c)–(8e).} \end{aligned} \quad (\text{EC.10})$$

Write $n^- + TP - TN = n^- + \sum_k 2^k \gamma_k^+ - \sum_l 2^l \gamma_l^-$ and linearize the products $FM2 \cdot \gamma^\pm$ via McCormick envelopes. Linearize TP^2 with ξ_{rs}^{++} . Model (EC.10) is equivalent to:

$$\begin{aligned} & \max FM2 \\ \text{s.t. } & FM2 \cdot (n^+ n^-) + n^+ \left(\sum_{k=0}^p 2^k \delta_k^+ - \sum_{l=0}^q 2^l \delta_l^- \right) \leq \sum_{r=0}^p \sum_{s=0}^p 2^{r+s} \xi_{rs}^{++} \\ \delta_k^+ = FM2 \cdot \gamma_k^+ \text{ via } & \begin{cases} \delta_k^+ \leq \gamma_k^+, \\ \delta_k^+ \leq FM2, \\ \delta_k^+ \geq FM2 - (1 - \gamma_k^+), \end{cases} \quad \forall k, \\ \delta_l^- = FM2 \cdot \gamma_l^- \text{ via } & \begin{cases} \delta_l^- \leq \gamma_l^-, \\ \delta_l^- \leq FM2, \\ \delta_l^- \geq FM2 - (1 - \gamma_l^-), \end{cases} \quad \forall l, \\ \xi_{rs}^{++} = \gamma_r^+ \wedge \gamma_s^+ \text{ via } & \begin{cases} \xi_{rs}^{++} \leq \gamma_r^+, \\ \xi_{rs}^{++} \leq \gamma_s^+, \\ \xi_{rs}^{++} \geq \gamma_r^+ + \gamma_s^+ - 1, \end{cases} \quad \forall r, s, \end{aligned} \quad (\text{EC.11})$$

(EC.8) and (8c)–(8e).

EC.4.4. Jaccard / Intersection-over-Union (IoU)

The IoU (also called Jaccard index) is

$$IoU = \frac{TP}{TP+FP+FN} = \frac{TP}{|\mathcal{I}| - TN}, \quad IoU \in [0, 1].$$

MIQCP.

$$\begin{aligned}
 & \max \text{IoU} \\
 \text{s.t. } & \text{IoU} \cdot (|\mathcal{I}| - \text{TN}) \leq \text{TP}, \\
 & \text{Constraints (5)–(6), (8c)–(8e).}
 \end{aligned} \tag{EC.12}$$

Expand $|\mathcal{I}| - \text{TN} = |\mathcal{I}| - \sum_l 2^l \gamma_l^-$ and linearize $\text{IoU} \cdot \gamma_l^-$ with McCormick envelopes. Model (EC.12) is equivalent to:

$$\begin{aligned}
 & \max \text{IoU} - \lambda \sum_{n \in \mathcal{B}} \sum_{f \in \mathcal{F}} b_{nf} \\
 \text{s.t. } & \text{IoU} \cdot |\mathcal{I}| - \sum_{l=0}^q 2^l \delta_l^- \leq \sum_{i \in \mathcal{U}: y_i=1} w_i g^i \\
 & \delta_l^- = \text{IoU} \cdot \gamma_l^- \text{ via } \begin{cases} \delta_l^- \leq \gamma_l^-, \\ \delta_l^- \leq \text{IoU}, \\ \delta_l^- \geq \text{IoU} - (1 - \gamma_l^-), \end{cases} \quad \forall l,
 \end{aligned} \tag{EC.13}$$

(EC.8) and (8c)–(8e).

EC.4.5. Diagnostic Odds Ratio (DOR)

The diagnostic odds ratio is

$$\text{DOR} = \frac{\text{TP} \cdot \text{TN}}{\text{FP} \cdot \text{FN}} = \frac{\text{TP} \cdot \text{TN}}{n^+ n^- - n^+ \text{TN} - n^- \text{TP} + \text{TP} \cdot \text{TN}}.$$

Because DOR can be unbounded when FP or FN equals 0, an exact MIP needs either (i) a modeling upper bound \bar{D} on DOR, or (ii) a small denominator smoothing $\varepsilon > 0$. We provide both variants.

Variant A (bounded DOR). Assume a user-specified bound $\bar{D} > 0$ (e.g., from validation or domain knowledge) and constrain $0 \leq \text{DOR} \leq \bar{D}$.

$$\begin{aligned}
 & \max \text{DOR} - \lambda \sum_{n \in \mathcal{B}} \sum_{f \in \mathcal{F}} b_{nf} \\
 \text{s.t. } & \text{DOR} \left[n^+ n^- - n^+ \text{TN} - n^- \text{TP} + \text{TP} \cdot \text{TN} \right] \leq \text{TP} \cdot \text{TN}, \\
 & 0 \leq \text{DOR} \leq \bar{D}, \\
 & \text{Constraints (5)–(6), (8c)–(8e).}
 \end{aligned} \tag{EC.14}$$

Expand the bracketed term linearly in γ^\pm and η_{kl} ; linearize the products $\text{DOR} \cdot \gamma^\pm$ and $\text{DOR} \cdot \eta_{kl}$ via McCormick with upper bound \bar{D} . Under $0 \leq \text{DOR} \leq \bar{D}$, (EC.14) is equivalent to:

$$\begin{aligned}
 & \max \text{DOR} - \lambda \sum_{n \in \mathcal{B}} \sum_{f \in \mathcal{F}} b_{nf} \\
 \text{s.t. } & \text{DOR} \cdot n^+ n^- - n^+ \sum_{l=0}^q 2^l \delta_l^- - n^- \sum_{k=0}^p 2^k \delta_k^+ + \sum_{k=0}^p \sum_{l=0}^q 2^{k+l} \zeta_{kl} \leq \sum_{k=0}^p \sum_{l=0}^q 2^{k+l} \eta_{kl} \\
 & \delta_k^+ = \text{DOR} \cdot \gamma_k^+ \text{ via } \begin{cases} \delta_k^+ \leq \bar{D} \gamma_k^+, \\ \delta_k^+ \leq \text{DOR}, \\ \delta_k^+ \geq \text{DOR} - \bar{D}(1 - \gamma_k^+), \end{cases} \quad \forall k, \\
 & \delta_l^- = \text{DOR} \cdot \gamma_l^- \text{ via } \begin{cases} \delta_l^- \leq \bar{D} \gamma_l^-, \\ \delta_l^- \leq \text{DOR}, \\ \delta_l^- \geq \text{DOR} - \bar{D}(1 - \gamma_l^-), \end{cases} \quad \forall l, \\
 & \zeta_{kl} = \text{DOR} \cdot \eta_{kl} \text{ via } \begin{cases} \zeta_{kl} \leq \bar{D} \eta_{kl}, \\ \zeta_{kl} \leq \text{DOR}, \\ \zeta_{kl} \geq \text{DOR} - \bar{D}(1 - \eta_{kl}), \end{cases} \quad \forall k, l, \\
 & \eta_{kl} = \gamma_k^+ \wedge \gamma_l^- \text{ as above,} \\
 & \text{(EC.8) and (8c)–(8e).}
 \end{aligned} \tag{EC.15}$$